

# Fluorophore-Induced Plasmonic Current: Generation-Based Detection of Singlet Oxygen

Rachael Knoblauch, Joshua Moskowicz, Elizabeth Hawkins, and Chris D. Geddes\*

Cite This: <https://dx.doi.org/10.1021/acssensors.0c00377>

Read Online

ACCESS |



Metrics &amp; More



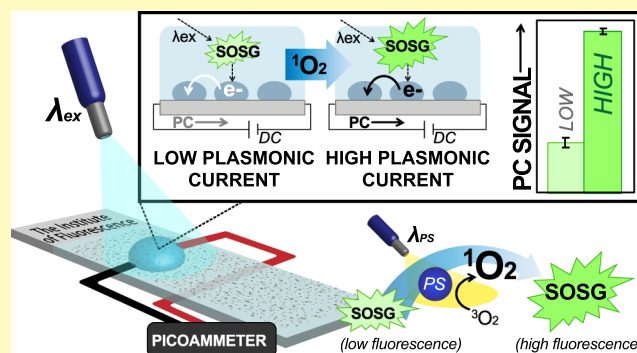
Article Recommendations



Supporting Information

**ABSTRACT:** In this work, we report the surface-based electrical detection of singlet oxygen using the emerging fluorophore-induced plasmonic current (PC) technique. By this method, we utilize the fluorescent “turn on” response of the well-known singlet oxygen sensor green (SOSG) singlet oxygen ( $^1\text{O}_2$ ) fluorescent probe for the generation of fluorophore-induced PC in a silver nanoparticle film. To demonstrate the potential utility of this new technique, a photosensitizing molecule is used to generate  $^1\text{O}_2$  in a solution containing the SOSG probe. The resulting change in SOSG fluorescence quantum yield and extinction coefficient permits stronger energy transfer from the SOSG probe to a proximal silver nanoparticle island film located in the near-electric field of the probe. This yields an increase in the induced electric current flow, allowing for the detection of the  $^1\text{O}_2$  analyte. To the author’s knowledge, this represents the first detection of the reactive oxygen species  $^1\text{O}_2$  utilizing fluorophore-induced PC methodology and even broader electrical detection of  $^1\text{O}_2$ . This is significant as it opens the possibility for  $^1\text{O}_2$  detection methods which do not require a traditional “photodetector” and associated optics, simplifying the instrumentation over existing fluorescence detection methods and potentially even lowering the cost.

**KEYWORDS:** plasmonic current, plasmonic electricity, plasmonics, reactive oxygen species, singlet oxygen, singlet oxygen sensor green, fluorescence detection, sensing



Reactive oxygen species (ROS) such as superoxide anion radical, hydroxyl radical, hydrogen peroxide, and notably singlet oxygen ( $^1\text{O}_2$ ) have implications and impact in a broad array of fields, with perhaps the strongest interest lying in health and medicine.<sup>1–3</sup> These species are derived from molecular oxygen and are well known to have important roles in cell signaling and maintaining regular biological function, yet oxidative stress can be severely damaging to organic and biological materials.<sup>4,5</sup> As such, the sensing of ROS to monitor the health of systems is needed. Conversely, the deleterious properties of ROS have generated research interest in the controlled production of such species; technologies such as photodynamic therapy, for example, employ the targeted generation of ROS to inflict oxidative damage on cancer cells, thereby providing an additional treatment option in localized cancers.<sup>1,3</sup> Therefore, detection of ROS has been vital in research settings for some time.

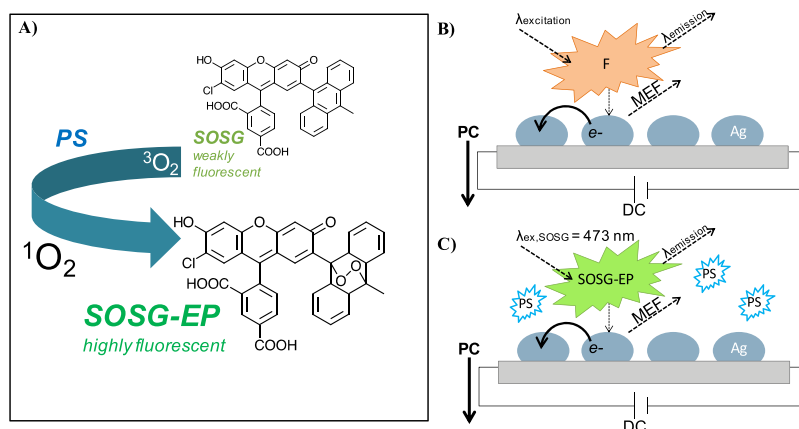
The generation of singlet oxygen is a key aspect of photodynamic therapies, and the mechanism of photosensitization includes the need for light-activated photosensitizing (PS) molecules to generate this species.<sup>6</sup> In brief, photosensitizers absorb light and undergo intersystem crossing to the triplet excited state; from this point, the molecule may relax via typical pathways such as radiative decay or interact with ground state molecular oxygen to alter its electronic spin

state.<sup>6</sup> A number of detection methods for singlet oxygen have been employed. Direct detection of  $^1\text{O}_2$  is possible as the molecule phosphoresces at 1275 nm.<sup>7</sup> This signal is typically weak and also is only observable in real-time, requiring sensitive fluorescence detection equipment and the limitation of constant monitoring of the system for detection. As an alternative, researchers have developed fluorescent probes such as singlet oxygen sensor green (SOSG) for the irreversible detection of singlet oxygen in the visible spectral region.<sup>8–10</sup> This probe consists of a fluorescent fluorescein-based moiety, covalently modified to include an anthracene substituent, as shown in Scheme 1A. This molecule has a low quantum yield because of excited state quenching via a photo-induced electron transfer (PET) mechanism.<sup>11</sup> In the presence of  $^1\text{O}_2$ , SOSG forms an endoperoxide in its anthracene moiety, preventing PET quenching, resulting in a large increase in

Received: February 26, 2020

Accepted: April 3, 2020

Published: April 3, 2020

Scheme 1. Schematic for Detection Methods of Singlet Oxygen ( $^1\text{O}_2$ )<sup>a</sup>

<sup>a</sup>(A) Schematic demonstrating the turn-on detection of  $^1\text{O}_2$  by SOSG) including both the weakly fluorescent and reacted, highly fluorescent endoperoxide (SOSG-EP) structures. (B) Schematic of fluorophore induced plasmonic current set up, depicting excitation and subsequent nonradiative energy transfer from a fluorophore to metal nanoparticle islands. Electron flow is indicated, along with concurrently detected metal-enhanced fluorescence. The blue coloring represents a liquid solvent. Electrodes are in simultaneous contact with the metal film and solvent. [Redrawn from ref 12]. (C) Modification of the PC set up from (B) for detection of singlet oxygen. The PS molecules are included.

fluorescence emission, and permitting the subsequent detection of  $^1\text{O}_2$ .<sup>11</sup>

Both direct and fluorescence probe detection methods necessitate expensive and sensitive optical equipment, which is limiting in the case of wide-spread detection techniques, point-of-care testing, and in low resource settings. To address this limitation, herein, we investigate for the first time the use of an emerging phenomenon called plasmonic current (PC) or plasmonic electricity (PE) for the surface-based detection of  $^1\text{O}_2$ . Fluorophore-induced PC is generated when an excited fluorescent molecule nonradiatively transfers energy to a nearby metallic nanoparticle film, generating a measurable electrical current through the film (Scheme 1B).<sup>12</sup> The generated electrical current is due to electron transport between discrete metal nanoparticles in the film, also known in the literature as electron “hopping” or “tunneling” for closely spaced particles.<sup>13–17</sup> The ability of nanoparticles in the film to support electron transport is dependent on the charging energy required for a nanoparticle to gain an electron, which is related to the particle capacitance, that is,

$$E_C = \frac{e^2}{2C} \quad (1)$$

where  $E_C$  is charging energy,  $e$  is the elementary electric charge, and  $C$  is capacitance of the particle.<sup>13–16</sup>

We have previously modeled the metal nanoparticle capacitance in our films utilizing the concentric sphere model for nanoparticle capacitance, which is a commonly used approach throughout the literature,<sup>16,18–21</sup>

$$C = 4\pi\epsilon_0\epsilon_r(r_0 + s)/s \quad (2)$$

where  $\epsilon_0$  is the vacuum permittivity,  $\epsilon$  is the relative permittivity of the medium surrounding the particle,  $r_0$  is the particle radius, and  $s$  is the distance between two neighboring particles. Upon excitation of a proximal fluorophore, energy transfer to the metal is expected to help overcome the coulombic gap to electron transport, increasing electron transport in the film. Previous work from our laboratory has demonstrated the effect of particle size and spacing in the fluorophore-induced current. Here, it was found that larger and

more closely spaced particles lead to an increase in particle capacitance and a decrease in the coulombic gap required for electron transport, providing for increased current generation with fluorophore excitation.<sup>22</sup> In addition, changing the particle size will cause a shift in the plasmon resonance frequency of the particle; however, this effect on the current is currently thought to be minor compared to the change in particle capacitance with changing particle size. The strength of direct coupling between metal nanoparticles and far-field excitation light decreases as nanoparticles grow in size toward the wavelength of incoming radiation.<sup>23</sup> Representative scanning electron microscopy (SEM) images of metal nanoparticles in our films have been collected in previous work;<sup>12</sup> the particles are relatively large ( $\sim 50 \text{ nm}$  diameter) and only weakly couple with direct far-field excitation light. These nanoparticles may still couple strongly with local near field molecular emitters,<sup>24</sup> generating an increase in electrical current through the film.

As described in recent work by our laboratory, this electrical current is dependent on a number of factors including not only nanoparticle size and spacing in the film but also solvent permittivity, applied voltage, temperature, and the fluorophore extinction coefficient.<sup>12,22</sup> In our studies of extinction coefficient effects, an increase in the current was observed with increasing fluorophore extinction coefficient.<sup>12</sup> This is thought to be due to the high extinction fluorophore absorbing more radiative energy from the far-field light (laser or LED) and bringing more energy into the near-electric field of the nanoparticles. Assuming no change in the fluorophore quantum yield, this leads to more energy transfer from the molecule to the metal and a subsequent increase in electron transport through the film. In a similar manner to fluorescence resonance energy transfer, we predict that a lower quantum yield will diminish energy transfer from the fluorophore to the metal, decreasing the observed induced PC. Essentially, the induced current is dependent on the fluorophore brightness, that is,

$$\text{Brightness} = \Phi_{\text{fl}}\epsilon_{\text{fl}} \quad (3)$$

where  $\Phi_{\text{fl}}$  is the fluorophore quantum yield and  $\epsilon_{\text{fl}}$  is the extinction coefficient.<sup>25</sup> In other words, the induced current in the nanoparticle film contains photophysical information pertaining to the fluorophore. This provides for a molecular fingerprint, opening the possibility for detection assays which distinguish species based on a change in extinction coefficient and quantum yield, as compared to actual radiative emission from a traditional fluorophore. This is significant as it represents a low-cost analytical method that does not require a photodetector and associated optics, thereby simplifying instrumentation over existing  $^1\text{O}_2$  spectrophotometric detection methods.

In this manuscript, we describe the utilization of the SOSG singlet oxygen probe as a molecular energy donor for PC generation on a silver nanoparticle substrate, expanding beyond its intended capacity as a fluorescence-on probe. It is clear that long-term use of silver films for biological sensing applications would not be preferred to substrates such as gold, which are superior in stability. In this instance, silver films were chosen due to their simplicity of fabrication and the significant overlap between the silver nanoparticle films' extinction spectra and the emission profile of the commercially available SOSG fluorescent probe. In addition, the relatively large size of the particles ( $\sim 50$  nm from SEM)<sup>12</sup> confer additional stability that is not inherent to smaller sized silver particles. Upon excitation of the SOSG molecule with far-field light (laser or LED), energy is readily transferred to the metal nanoparticle film, allowing for the generation of PC (Scheme 1C). In the presence of  $^1\text{O}_2$ , generated by the light activation of the photosensitizer (PS), SOSG displays a change in fluorescence brightness because of an alteration of both extinction coefficient and fluorescent quantum yield, which is expected to result in an increased PC as compared to SOSG without  $^1\text{O}_2$  exposure. We subsequently investigated the detection of  $^1\text{O}_2$  via the SOSG induced PC, an unreported sensing modality until now.

## MATERIALS AND METHODS

**Silver Nanoparticle Island Film Preparation: Thermal Vapor Deposition.** Silver nanoparticle island films were prepared using thermal vapor deposition and silver pellets (99.999%, Research and PVD Materials Corporation), as described in previous work from our laboratory.<sup>12</sup> Briefly, silane-prep glass microscope slides (Sigma-Aldrich) were first cleaned with methanol and dried under  $\text{N}_2$ ; these were subsequently used as a substrate for vapor deposition using an Edwards BOC Auto 306 Vapor Deposition Unit, at a pressure of  $9 \times 10^{-6}$  Torr. The deposition rate was held constant at  $0.1 \text{ \AA/s}$  with a deposition time of 28 min. Prepared films were cooled to room temperature and stored in a desiccator under vacuum until use.

**Silver Nanoparticle Film Characterization.** Silver nanoparticle island films utilized for SOSG induced current measurements were characterized, as described in a previous manuscript from our laboratory.<sup>12</sup> Briefly, absorption spectra of prepared silver films were collected using a single beam Varian Cary 50-Bio UV–VIS spectrophotometer. SEM of vapor deposited films was performed using a Nova NanoSEM 450 with secondary electron imaging, with representative film surface images displayed in previous work.<sup>12</sup> All dry silver nanoparticle island films were characterized as electrically noncontinuous, displaying zero measurable current under zero applied bias voltage.<sup>22</sup>

**Instrumentation.** Fluorescence and absorption measurements of rose bengal and methylene blue (Sigma-Aldrich) solutions were performed in a quartz cuvette. Fluorescence was measured using a Fluoromax-4P spectrophotometer; absorption spectra were collected using the Varian Cary 50-Bio UV–VIS spectrophotometer, as mentioned previously. Electrical current through the system was

measured with a Keithley 6487 picoammeter, in either an open circuit configuration or under an applied potential, with digital output to an external computer, as described previously.<sup>12</sup> Electrode materials were selected to match the metal nanoparticle film (e.g., silver-on-silver). The electrodes were positioned to make simultaneous contact with the metal nanoparticle film and the liquid solvent. Conductivity measurements were carried out with a Fisher Scientific Accumet Conductivity Meter.

**Photosensitization of SOSG and Induced PC Measurements.** In order to determine the detectability of  $^1\text{O}_2$  using SOSG induced PC measurements, solutions of SOSG were first prepared by performing various dilutions of stock SOSG (5 mM) with methylene blue, previously prepared in de-ionized water to known concentrations. To perform the photosensitization step, the solutions were divided into two aliquots (Scheme S1); one aliquot was transferred to a black centrifuge tube and received no light exposure, thereby avoiding photosensitization. The other aliquot was added to a  $500 \mu\text{L}$  quartz cuvette, capped, and exposed to white light using a ThorLabs OSL1 fiber illuminator. Following exposure, the aliquot was transferred to a black centrifuge tube for PC detection.

Following photosensitization, aliquots were pipetted onto an electrically noncontinuous silver nanoparticle island film and allowed to diffuse into the gaps between separate nanoparticle islands. Upon addition of solution to the metal, electrical current due to fluorophore convection was allowed to stabilize for approximately 5 min. Both photosensitized and control solutions were then excited with a 473 nm LED directed at the film surface. Change in electrical current through the fluorophore-metal system was monitored in an open circuit configuration at room temperature ( $20 \text{ }^\circ\text{C}$ ) and reported as the absolute value of current change,  $\Delta I$ , with application of the excitation source. This method of reporting accounts for any background current that may already be inherent to the system, for example, due to ions in solution. Similarly, background current changes are monitored with application of the excitation in the absence of the fluorophore; this background may be subtracted from the fluorophore-induced signal. Statistical analysis of all results reported herein are the result of a minimum of  $n = 3$  measurements and were performed using Student's *T*-test, assuming equal variances. Model fits and corresponding equations and values were determined using the LINEST function in Microsoft Excel.

## RESULTS AND DISCUSSION

### Role of Photosensitizer in Fluorophore-Induced PC.

In order to generate the highly fluorescent endoperoxide form of SOSG, a photosensitizer molecule is required to first produce  $^1\text{O}_2$  (Scheme 1). Rose bengal and methylene blue are two well-known  $^1\text{O}_2$  photosensitizers and were both therefore considered for this proof-of-concept study.<sup>26</sup> Both photosensitizers absorb in the visible region (Figure 1a) and therefore can generate  $^1\text{O}_2$  via white light exposure. It is also desirable for the photosensitizer to not be excited by the SOSG excitation source (473 nm LED), as this could lead to energy transfer from the photosensitizer itself to the nanoparticles, potentially causing background interference in the SOSG-induced PC. Figure 1a shows the normalized absorption spectra of both photosensitizers; methylene blue shows less overlap with the LED source emission spectrum as compared to rose bengal; at 473 nm, the extinction coefficient of the latter ( $\epsilon_{\text{RB},473} = 6200 \pm 100 \text{ M}^{-1} \text{ cm}^{-1}$ ,  $n = 3$ ) is considerably higher than that of the former ( $\epsilon_{\text{MB},473} = 1600 \pm 600 \text{ M}^{-1} \text{ cm}^{-1}$ ,  $n = 4$ . Figure S1). This opens the possibility for excitation of rose bengal during PC detection and subsequent background rose bengal current interference in the desired SOSG-induced electrical signal. This is observable also in the fluorescence emission spectra of each photosensitizer when excited at 473 nm; while emission from rose bengal is detectable in the combined solution of SOSG and rose bengal

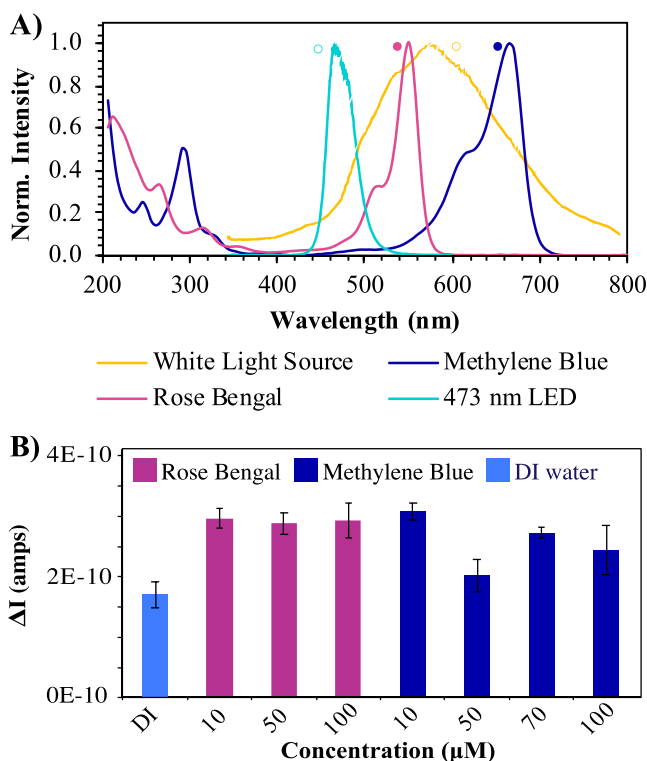


**Figure 1.** Determination of optimal photosensitizer for singlet oxygen ( $^1\text{O}_2$ ) detection using PC. (A) Normalized absorption spectra (closed circles) of rose bengal and methylene blue overlaid with the emission spectra (open circles) of the white light source (photosensitization) and PC excitation source (473 nm LED). (B) Change in current detected upon excitation of photosensitizer solutions at 473 nm.

photosensitizer, methylene blue does not emit in the wavelength region of interest for SOSG (Figure S2). Based on these photophysical data, methylene blue is the preferred photosensitizer for SOSG-induced PC detection of  $^1\text{O}_2$  for our application.

In addition to the aforementioned considerations, changes in the relative permittivity of the solution matrix (i.e., PS solution) used in PC analysis were also investigated, as a change in the relative permittivity of the medium surrounding the nanoparticle can alter the charging energy and particle capacitance required for electron transport according to eqs 2 and 3, respectively. In other words, the background signal (noise) in the fluorophore-induced PC measurement is affected by a change in solution dielectric constant, which may occur in the presence of the photosensitizer molecule. Therefore, the induced current with methylene blue in the absence of the SOSG analyte was monitored (Figure 1b). The conductivity of methylene blue was also measured in order to better understand the change in dielectric constant responsible for the induced background signal (Figure S3). While both methylene blue and rose bengal induced a greater current than DI water alone, the background signal between photosensitizers was not significantly different, indicating that either a photosensitizer may be considered a reasonable choice for the SOSG-induced plasmonic detection of  $^1\text{O}_2$ . Based on these measurements and photophysical properties, methylene blue was chosen as the photosensitizer for all subsequent experiments; 50  $\mu\text{M}$  solutions were chosen based on the favorable low background current shown in Figure 1b.

### Detection of Singlet Oxygen via SOSG-Induced PC.

SOSG is known to detect  $^1\text{O}_2$  because of a significant quantum yield increase following reaction with  $^1\text{O}_2$ , with reported values of 0.009 and 0.45 for unreacted SOSG and the endoperoxide, respectively.<sup>11</sup> In the low quantum yield state, intramolecular PET in the SOSG molecule from the anthracene to fluorescein moieties prevents relaxation via fluorescence emission.<sup>11</sup> After  $^1\text{O}_2$  photosensitization and endoperoxide formation, the relative energies of the highest occupied molecular orbital and lowest unoccupied molecular orbital of each moiety are altered and PET is no longer favorable; radiative decay therefore becomes a competitive relaxation pathway. In a modality similar to its fluorescent function, this increase in brightness ultimately leads to the increase in the induced PC. Quantum yield change in the probe alone is not the only potential mechanism for  $^1\text{O}_2$  detection via SOSG-induced PC. Given that the mechanism of  $^1\text{O}_2$  detection involves chemical modification of the probe itself, a change in ground state properties is possible. Similar to another report on SOSG,<sup>27</sup> we have observed an increase in extinction of SOSG after photosensitization, when the endoperoxide is formed in solution<sup>a</sup> (Figure 2, Table S1).

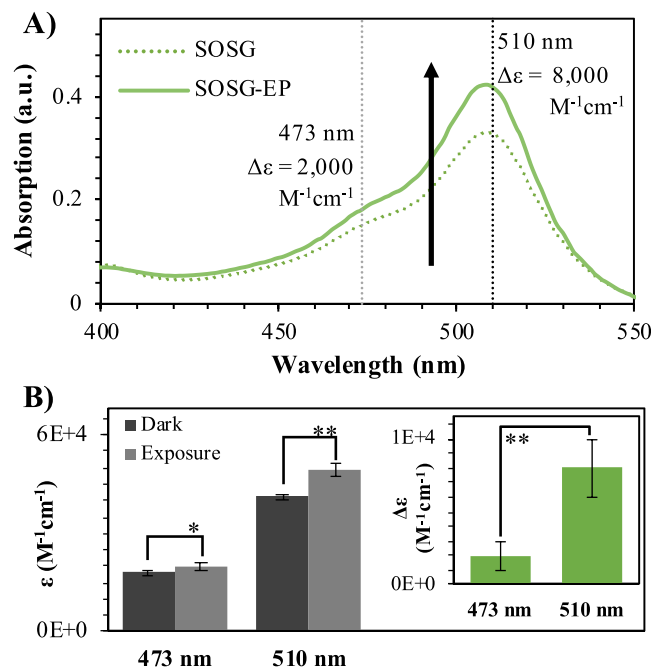


**Figure 2.** Absorption of SOSG (20  $\mu\text{M}$ ) before and after formation of the endoperoxide<sup>a</sup> (SOSG-EP) postexposure to white light (10 min) with 50  $\mu\text{M}$  Methylene blue. (A) Absorption spectra. Wavelengths of interest are reported with the corresponding extinction coefficient changes from exposure ( $\Delta\epsilon_{473} = 2000 \pm 1000 \text{ M}^{-1} \text{ cm}^{-1}$ ,  $\Delta\epsilon_{510} = 8000 \pm 2000 \text{ M}^{-1} \text{ cm}^{-1}$ ) (B) calculated extinction coefficients at each wavelength of interest and resulting statistical analysis using a *T*-test assuming equal variance. Inset displays the change in extinction coefficient. Error is from standard deviation of  $n = 5$  trials. \* $p < 0.10$  (90% confidence) and \*\* $p < 0.001$  (99.9% confidence).

Before photosensitization, the extinction coefficient of SOSG at 473 nm is  $18,000 \pm 1000 \text{ M}^{-1} \text{ cm}^{-1}$ , a value >10-fold greater than methylene blue. Previous reports from our lab have shown PC detection of fluorophores to be much more favorable for molecules with higher extinction values,<sup>12</sup> indicating that SOSG induced detection has the potential to

be discernible from the methylene blue background. Because the extinction coefficient of photosensitized SOSG increases by 11% relative to the “dark” solution ( $\Delta\epsilon_{473} = 2000 \pm 1000 \text{ M}^{-1} \text{ cm}^{-1}$ ), by extinction values alone, we could predict  $^1\text{O}_2$  detection via SOSG-induced PC should be possible.

To determine optimal experimental parameters for SOSG-induced plasmonic detection of  $^1\text{O}_2$ , we first prepared a series of SOSG solution concentrations in 50  $\mu\text{M}$  methylene blue. Each solution was exposed to white light for 10 min in a closed system, as described in previous sections, and the fluorescence emission detected, as shown in Figure 3. As expected, quantum

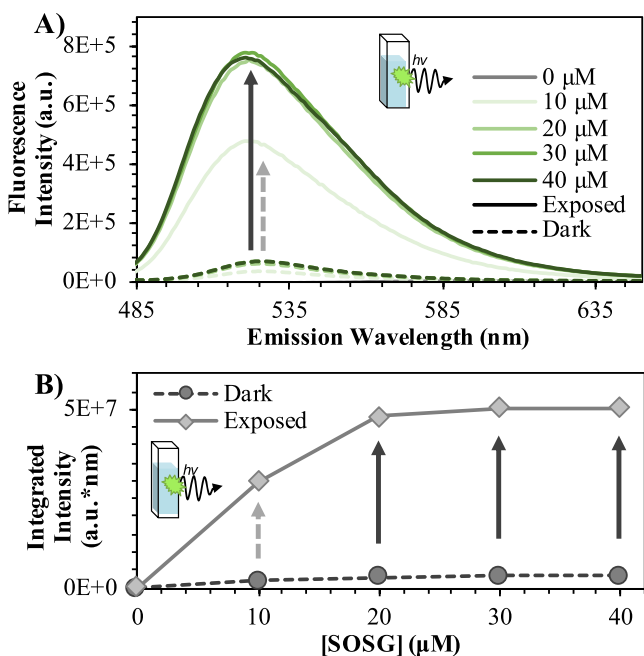


**Figure 3.** Fluorescence detection of singlet oxygen ( $^1\text{O}_2$ ) using SOSG at varying concentrations. (A) Fluorescence spectra of each probe concentration both pre (“dark,” dashed lines) and postexposure (“exposed,” solid lines) to white light for 10 min in a closed system. (B) Integrated intensities ( $\lambda_{\text{emission}} = 485\text{--}650 \text{ nm}$ ) of SOSG emission pre and postexposure. Arrows indicate signal increase after photosensitization (exposure).

yield increases are observed in the exposed versus dark solutions. This effect appears concentration dependent for 10 versus 20  $\mu\text{M}$  solutions but plateaus at higher concentrations of SOSG. This is likely due to the closed nature of the experimental system; in this case, molecular oxygen rather than SOSG is the limiting reagent. These SOSG concentrations were subsequently tested for PC generation to minimize background current generated from unreacted SOSG.

Having established the parameters, the photosensitized solutions were then analyzed using the surface-based PC detection method on silver nanoparticle film substrates. Figure 4 demonstrates the fluorophore-induced current increase between the low-fluorescence (“dark” conditions with no  $^1\text{O}_2$  generation) and high-fluorescence (“exposure” conditions leading to  $^1\text{O}_2$  generation and endoperoxide formation) forms of SOSG at varying concentrations. While a photosensitizer-containing control solution without SOSG displayed no significant difference in the induced current when exposed to the  $^1\text{O}_2$  generation source, a 20  $\mu\text{M}$  SOSG solution was found to display a very large (228%) current increase in the presence of  $^1\text{O}_2$ . This 228% increase in the induced electrical signal is correlated with an increase in fluorescence brightness (Figures 4 and S4).

These results are most significant, as they demonstrate the utility of the fluorophore-induced PC platform in the detection of singlet oxygen via the large “turn on” fluorescence response of the SOSG molecular probe. We were subsequently curious if the exposure time dependence of photosensitization could be monitored using SOSG-induced PC detection. Figure 5 shows the induced plasmonic current with varying exposure time, using a concentration of 20  $\mu\text{M}$  SOSG and 50  $\mu\text{M}$  methylene blue as the photosensitizer. Here, as the white light exposure time is increased for the photosensitizer, more  $^1\text{O}_2$  is generated. This increase ultimately leads to a greater number of SOSG molecules in the highly fluorescent, endoperoxide form. Figure 5a shows the corresponding increase in fluorescence intensity, which progresses in a linear fashion (Figure S5). Figure 5b shows the correlation in the induced current, which displays a positive and also linear trend with increasing exposure time with an approximate 3-fold increase in signal over 600 s of exposure (statistical analysis in Figure S6, Table S2). The successful detection of  $^1\text{O}_2$  using SOSG-induced plasmonic current described herein reinforces the vast

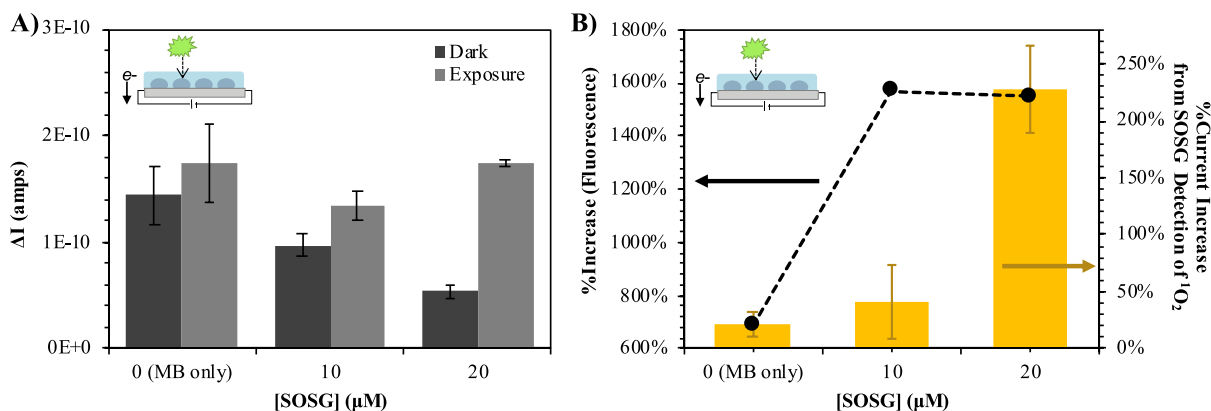


**Figure 4.** Detection by PC of singlet oxygen ( $^1\text{O}_2$ ) photosensitized with methylene blue (50  $\mu\text{M}$ ) and white light for 10 min in a closed system using SOSG at varying concentrations. (A) Detected PC change ( $\Delta I$ ) for each solution upon excitation (473 nm LED). Both pre (“dark”) and post (“exposure”) photosensitization solutions were measured. (B) Percent increase in the PC signal plotted against the percent increase in fluorescence integrated intensity for each concentration of SOSG postexposure. Error is from the standard deviation of  $n = 3$  measurements.

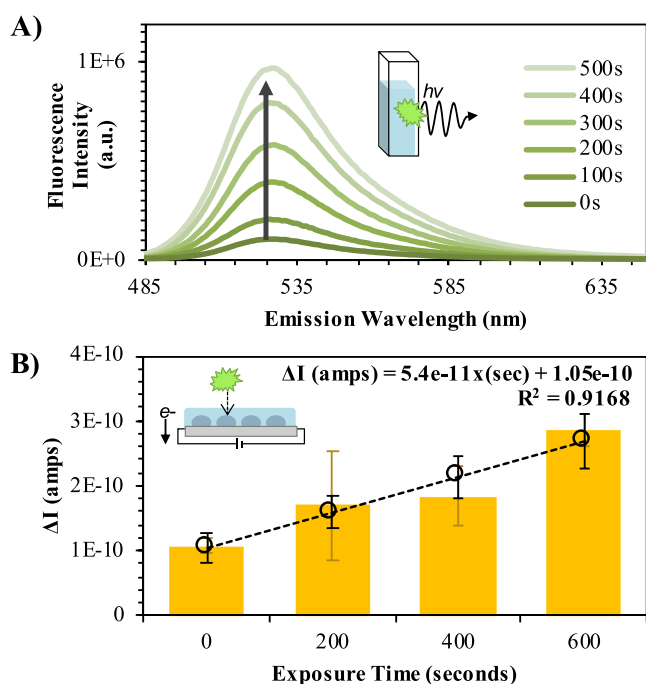


**Figure 5.** Detection of singlet oxygen ( $^1\text{O}_2$ ) by SOSG ( $20\ \mu\text{M}$ ) photosensitized with methylene blue ( $50\ \mu\text{M}$ ) and white light for varying exposure time intervals. (A) Fluorescence spectra. (B) PC increase with 473 nm LED excitation, detected after photosensitization. Error is from the standard deviation of  $n \geq 3$  measurements. The linear model fit is also plotted with model error for each time point, the model equation, and  $R^2$  value.

potential that this surface detection method may exhibit in future applications.

## CONCLUSIONS

Herein, we have reported the successful detection of singlet oxygen using the novel phenomenon of fluorophore-induced plasmonic current (PC). Singlet oxygen was detected using the well-known fluorescence-on probe SOSG, which in turn was able to induce plasmonic current in silver island films, which was then detected by an ammeter. Both an increase in extinction coefficient and quantum yield associated with the mechanism of singlet oxygen detection by SOSG are implicated as favorable properties for the use of fluorescent probes in plasmonic current-based detection applications. The results reported herein provide a promising foundation for future development of probes specific to plasmonic current in a new chapter of detection and sensing research. Future sensing fluorophores developed specifically for induced plasmonic current will potentially require metal films beyond silver, depending on their extinction/fluorophore emission spectral properties. This aspect opens the door for optimization of substrate characteristics—including stability for long-term or repeated use—as the field develops. In terms of ROS detection, it is interesting to note that generation of singlet oxygen has no considerable impact on the absorption properties of silver island films used in this study (Figure S7, Table S3). The fact that these substrates are stable in the presence of such highly reactive species provides further support for their use in future sensing applications such as plasmonic current. Described herein is only one example of how fluorescence-induced plasmonic current may be used in sensing applications. Plasmonic current detection bypasses the

need for traditional optics, reducing the cost and footprint associated with traditional fluorescence detection and microscopy methods. The simplicity of plasmonic current could serve to reduce the cost of detection devices, simplify design for innovative point-of-care testing, and broaden the scope of sensing capabilities beyond what is currently possible using fluorescence detection methods. Implications of plasmonic current extend far beyond ROS into fields from quality control to diagnostics.

## ASSOCIATED CONTENT

### Supporting Information

The Supporting Information is available free of charge at <https://pubs.acs.org/doi/10.1021/acssensors.0c00377>.

Diagram of the experimental procedure, absorption intensities of methylene blue and rose bengal photosensitizers of varying concentrations, normalized fluorescence spectra of SOSG ( $20\ \mu\text{M}$ ), conductivity values of methylene blue solutions in deionized (DI) water, extinction Coefficients ( $\epsilon$ ) of SOSG solutions at different wavelengths, statistical analysis ( $T$ -test, equal variance) of detection by plasmonic current of singlet oxygen ( $^1\text{O}_2$ ) photosensitized with methylene blue ( $50\ \mu\text{M}$ ) and white light, fluorescence detection of singlet oxygen ( $^1\text{O}_2$ ) by SOSG ( $20\ \mu\text{M}$ ) photosensitized with methylene blue ( $50\ \mu\text{M}$ ) and white light, statistical analysis for plasmonic current (PC) detection of singlet oxygen ( $^1\text{O}_2$ ) by SOSG ( $20\ \mu\text{M}$ ) photosensitized with methylene blue (MB,  $50\ \mu\text{M}$ ) and white light, confidence intervals for statistical analysis of singlet oxygen detection by plasmonic current, absorption spectra of Silver Island Films on glass substrates, and changes in spectral properties of silver island films following exposure to variation solution conditions (PDF)

## AUTHOR INFORMATION

### Corresponding Author

Chris D. Geddes – Institute of Fluorescence and Department of Chemistry and Biochemistry, University of Maryland, Baltimore County, Baltimore, Maryland 21202, United States; Phone: (410) 576-5723; Email: [geddes@umbc.edu](mailto:geddes@umbc.edu); Fax: (410) 576-5722

### Authors

Rachael Knoblauch – Institute of Fluorescence and Department of Chemistry and Biochemistry, University of Maryland, Baltimore County, Baltimore, Maryland 21202, United States; [orcid.org/0000-0001-9653-1823](https://orcid.org/0000-0001-9653-1823)

Joshua Moskowitz – Institute of Fluorescence and Department of Chemistry and Biochemistry, University of Maryland, Baltimore County, Baltimore, Maryland 21202, United States; [orcid.org/0000-0002-4768-9082](https://orcid.org/0000-0002-4768-9082)

Elizabeth Hawkins – Institute of Fluorescence and Department of Chemistry and Biochemistry, University of Maryland, Baltimore County, Baltimore, Maryland 21202, United States

Complete contact information is available at: <https://pubs.acs.org/doi/10.1021/acssensors.0c00377>

### Author Contributions

All experiments were designed and executed by J.M. and R.K. under the mentorship of C.D.G.. E.H. aided in the execution of

photosensitization procedures. The manuscript was written collaboratively by J.M. and R.K., edited by C.D.G.. J.M. and R. K. contributed equally to this work.

### Funding

This work was supported by the National Science Foundation Graduate Research Fellowship Program (2018262827), the HHS/NIH/National Institute of General Medical Sciences (NIGMS) through the Chemistry/Biology Interface Program at the University of Maryland Baltimore County (5T32GM066706), and the Institute of Fluorescence at the University of Maryland Baltimore County Internal Funding.

### Notes

The authors declare no competing financial interest.

## ACKNOWLEDGMENTS

The authors acknowledge the Institute of Fluorescence (IoF) and the Department of Chemistry and Biochemistry at the University of Maryland Baltimore County (UMBC) for financial support.

## ADDITIONAL NOTE

<sup>a</sup>The reported extinction coefficients are not meant to be analytical values for pure SOSG and pure SOSG-EP but are rather intended to demonstrate the photophysical effects following photosensitization of and reaction with singlet oxygen.

## REFERENCES

- (1) Patrice, T. *Photodynamic Therapy*; Royal Society of Chemistry: Cambridge, 2003.
- (2) Xiong, Y.; Tian, X.; Ai, H.-w. Molecular Tools to Generate Reactive Oxygen Species in Biological Systems. *Bioconjugate Chem.* **2019**, *30*, 1297–1303.
- (3) Baskaran, R.; Lee, J.; Yang, S.-G. Clinical development of photodynamic agents and therapeutic applications. *Biomater. Res.* **2018**, *22*, 25.
- (4) Dessauer, B. v.; Rodrigo, R. *Oxidative Stress and the Critically Ill Patient*; Nova Science Publishers, Inc: New York, 2012.
- (5) Chiueh, C. C.; Gilbert, D. L. *Reactive Oxygen Species: From Radiation to Molecular Biology: A Festschrift in Honor of Daniel L. Gilbert*; New York Academy of Sciences, 2000.
- (6) Kanofsky, J. R., Chapter 5: Photosensitization. In *Singlet Oxygen: Applications in Biosciences and Nanosciences*; Nonell, S., Flors, C., Eds.; Royal Society of Chemistry: Cambridge, 2016; Vol. 1, pp 95–103.
- (7) Boix-Garriga, E.; Rodríguez-Amigo, B.; Planas, O.; Nonell, S., Chapter 2: Properties of Singlet Oxygen. In *Singlet Oxygen: Applications in Biosciences and Nanosciences*; Nonell, S., Flors, C., Eds.; Royal Society of Chemistry: Cambridge, 2016; Vol. 1, pp 25–46.
- (8) Price, M.; Reiners, J. J.; Santiago, A. M.; Kessel, D. Monitoring Singlet Oxygen and Hydroxyl Radical Formation with Fluorescent Probes during Photodynamic Therapy. *Photochem. Photobiol.* **2009**, *85*, 1177–1181.
- (9) Driever, S. M.; Fryer, M. J.; Mullineaux, P. M.; Baker, N. R., Imaging of Reactive Oxygen Species In vivo. In *Plant Signal Transduction: Methods and Protocols*; Pfanschmidt, T., Ed.; Humana: New York, NY, 2009; pp 109–116.
- (10) Flors, C.; Fryer, M. J.; Waring, J.; Reeder, B.; Bechtold, U.; Mullineaux, P. M.; Nonell, S.; Wilson, M. T.; Baker, N.R. Imaging the production of singlet oxygen in vivo using a new fluorescent sensor, Singlet Oxygen Sensor Green. *J. Exp. Bot.* **2006**, *57*, 1725–1734.
- (11) Kim, S.; Fujitsuka, M.; Majima, T. Photochemistry of Singlet Oxygen Sensor Green. *J. Phys. Chem. B* **2013**, *117*, 13985–13992.
- (12) Moskowitz, J.; Geddes, C. D. Plasmonic Electricity: Fluorophore-Induced Plasmonic Current. *J. Phys. Chem. C* **2019**, *123*, 27770–27777.
- (13) Moore, R. G. C.; Evans, S. D.; Shen, T.; Hodson, C. E. C. Room-temperature single-electron tunnelling in surfactant stabilised iron oxide nanoparticles. *Phys. E* **2001**, *9*, 253–261.
- (14) Schmid, G. D. *Nanoparticles: From Theory to Application*; Wiley-VCH: Weinheim, c2004: 2004.
- (15) Markovich, G.; Collier, C. P.; Heath, J. R. Reversible Metal-Insulator Transition in Ordered Metal Nanocrystal Monolayers Observed by Impedance Spectroscopy. *Phys. Rev. Lett.* **1998**, *80*, 3807–3810.
- (16) Kano, S.; Tanaka, D.; Sakamoto, M.; Teranishi, T.; Majima, Y. Control of charging energy in chemically assembled nanoparticle single-electron transistors. *Nanotechnology* **2015**, *26*, 045702.
- (17) Negishi, R.; Hasegawa, T.; Tanaka, H.; Terabe, K.; Ozawa, H.; Ogawa, T.; Aono, M. Size-Dependent Single Electron Tunneling Effect in Au Nanoparticles. *Surf. Sci.* **2007**, *601*, 3907–3911.
- (18) Weaver, M. J.; Gao, X. Molecular Capacitance - Sequential Electron-Transfer Energies for Solution-Phase Metallic Clusters in Relation to Gas-Phase Clusters and Analogous Interfaces. *J. Phys. Chem.* **1993**, *97*, 332–338.
- (19) Garcia-Morales, V.; Mafé, S. Monolayer-Protected Metallic Nanoparticles: Limitations of the Concentric Sphere Capacitor Model. *J. Phys. Chem. C* **2007**, *111*, 7242–7250.
- (20) Li, D.; Li, J. Preparation, characterization and quantized capacitance of 3-mercapto-1,2-propanediol monolayer protected gold nanoparticles. *Chem. Phys. Lett.* **2003**, *372*, 668–673.
- (21) Wolfe, R. L.; Murray, R. W. Analytical Evidence for the Monolayer-Protected Cluster Au<sub>225</sub>[(S(CH<sub>2</sub>)SCH<sub>3</sub>)]<sub>75</sub>. *Anal. Chem.* **2006**, *78*, 1167–1173.
- (22) Moskowitz, J.; Sindi, R.; Geddes, C. D. Plasmonic Electricity II: The Effect of Particle Size, Solvent Permittivity, Applied Voltage, and Temperature on Fluorophore-Induced Plasmonic Current. *J. Phys. Chem. C* **2020**, *124*, 5780–5788.
- (23) Pelton, M.; Bryant, G. W. *Introduction to Metal-Nanoparticle Plasmonics*; John Wiley & Sons, Inc.: Hoboken, New Jersey, 2013.
- (24) Lakowicz, J. R. Radiative decay engineering 3. Surface plasmon-coupled directional emission. *Anal. Biochem.* **2004**, *324*, 153–169.
- (25) Lakowicz, J. R. *Principles of Fluorescence Spectroscopy*, 3rd ed.; Springer: New York, 2006.
- (26) Whitmire, C. *Photosensitizers: Types, Uses, and Selected Research*; Nova Science Publishers, Inc: Hauppauge, New York, 2016.
- (27) Ragàs, X.; Jiménez-Banzo, A.; Sánchez-García, D.; Batllori, X.; Nonell, S. Singlet oxygen photosensitisation by the fluorescent probe Singlet Oxygen Sensor Green. *Chem. Commun.* **2009**, 2920–2922.